AIP Journal of Applied Physics

Strong negative differential conductance in strained graphene devices

M. Chung Nguyen, V. Hung Nguyen, Huy-Viet Nguyen, and P. Dollfus

Citation: Journal of Applied Physics **118**, 234306 (2015); doi: 10.1063/1.4937911
View online: http://dx.doi.org/10.1063/1.4937911
View Table of Contents: http://scitation.aip.org/content/aip/journal/jap/118/23?ver=pdfcov
Published by the AIP Publishing

Strong negative differential conductance in strained graphene devices

M. Chung Nguyen,[1,2,a)] V. Hung Nguyen,[1,2] Huy-Viet Nguyen,[3,2,b)] and P. Dollfus[1]
[1]*Institut d'Electronique Fondamentale, CNRS, Univ. Paris Sud, Université Paris-Saclay, 91405 Orsay, France*
[2]*Center for Computational Physics, Institute of Physics, Vietnam Academy of Science and Technology, P.O. Box 429 Bo Ho, 10000 Hanoi, Vietnam*
[3]*Institute of Research and Development, Duy Tan University, K7/25 Quang Trung, Danang, Vietnam*

(Received 15 October 2015; accepted 2 December 2015; published online 17 December 2015)

In this work, we investigate the transport properties of devices made of graphene strained heterochannels. Due to the effects of local strain on the band structure, the Klein tunneling is strongly suppressed and transport gaps can appear in the unstrained/strained graphene junctions. The gap regions can be modulated in *k*-space and in energy by strain and doping engineering, respectively. We show that these effects can be exploited to achieve a strong negative differential conductance (NDC) in single gate-induced barrier structures and in p–n junctions. When the local strain is suitably applied, the peak-to-valley ratio (PVR) of the current-voltage characteristics can be as high as a few hundred. The dependence of NDC effect on structure parameters is investigated systematically. In particular, a strong NDC is obtained in single barrier structures with large strained region, while the PVR is not strongly sensitive to the transition length in p–n junctions.
 [http://dx.doi.org/10.1063/1.4937911]

I. INTRODUCTION

Beyond the usual linear or saturation behaviors expected to occur in transistors, non-linear effects as negative differential conductance (NDC) in the current-voltage characteristics may be of strong interest to design devices for high-speed analog applications and memories.[1] Hence, a lot of works have been devoted recently to investigate the possibility to generate a negative differential conductance or a transconductance in graphene devices, based on various physical mechanisms.

For 2D graphene sheets, a NDC behavior has been observed experimentally in graphene transistors[2–5] and explained theoretically as a possible consequence of chiral tunneling regime.[6,7] However, the effect is relatively weak due to the gapless character of graphene. The gapless band structure leads to the fact that the band-to-band tunneling can give important contributions to the current, making the valley current relatively high.[8,9] Recently, a strong NDC effect has been demonstrated in graphene/boron nitride/graphene van der Waals heterostructures in resonant tunneling regime.[10–12] A NDC behavior can be also obtained in tunnel diodes by controlling the interband tunneling between the conduction band of the n-doped side and the valence band in the p-doped side of the junction. Though small in gapless monolayer and bilayer graphene sheets,[13] this effect increases significantly if a finite bandgap can be generated in graphene, as discussed below. The NDC has been predicted also in double-barrier resonant tunneling diodes,[14–16] in diodes made of graphene/boron nitride heterochannels,[17] and in graphene nanoribbon (GNR) superlattices with different ballistic transport regimes, including the resonant tunneling through the minibands and the Wannier-Stark ladder regime.[18]

Nanostructuring graphene into nanoribbons offers promising possibilities to enhance non-linear effects in the *I-V* characteristics. The NDC effect has been predicted in different kinds of armchair GNRs working in resonant tunneling regime[19,20] and in heterochannels made of GNR sections with different widths.[21,22] The effect of parity selective rule[23] in zigzag GNRs with an even number of zigzag lines has been also predicted to generate a NDC behavior.[24] Regardless of the width of zigzag GNR, the mismatch of modes between left and right sides of a zigzag GNR junction may also induce a NDC.[25,26] Actually, the strongest NDC effect, with high peak-to-valley ratio (PVR) of several hundred, has been predicted to occur in tunnel diodes made of GNR heterochannels with alternating sections of different widths.[27] This large PVR is essentially due to a bandgap nanoengineering to enhance the peak current. Another graphene nanostructure, i.e., nanomesh lattices, has been also demonstrated as a good channel for NDC devices.[28]

In this paper, we explore a new possibility to generate a strong NDC effect in graphene devices by exploiting the transport gap that can arise at strained/unstrained graphene junctions. It has been experimentally demonstrated that a 2D graphene sheet is conformable and able to sustain large strain of over 20%.[29] Therefore, modifying the electronic structure of this material by strain engineering has been proposed as an alternative approach to overcome the lack of bandgap in graphene. In a recent work,[30] we have investigated the effects of uniaxial strain on the transport properties of 2D graphene strained/unstrained heterochannels and found that a significant transport gap of a few hundred meV can be achieved with a small strain of a few percent. This transport gap is not due to a bandgap opening in the band structure but due to the strain-induced shift of the Dirac cones in the Brillouin zone of different graphene sections. These results motivated us to study here the possibility of enhancing NDC behavior by local strain in graphene nanodevices, i.e., single

a)mai-chung.nguyen@u-psud.fr
b)nhviet@iop.vast.ac.vn

potential barrier structure and p–n tunnel diode. Actually, different techniques to generate local strains at the nanoscale in graphene and 2D materials have been explored.[31–37] For instance, a scalable process capable of generating local strains in graphene by laser-induced shock pressure has been demonstrated.[35] With this technique, the strain takes place in a circular mold, the size of which is related to the strain amplitude. It turns out that a strain of a few percent can be achieved in molds of size in the range from 50 to a few hundred nm. This is the typical size of strain area in the device channels studied here. We will show that in the considered devices, the PVR can reach high values, i.e., a few hundred. Additionally, in the case of a p–n tunnel diode, this ratio is shown to be not strongly sensitive to the transition length, i.e., the length of the region across which the charge density changes monotonically from n-type to p-type, which is usually difficult to control.

II. MODEL AND CALCULATIONS

In this work, we investigate the possibility to obtain a strong NDC behavior in 2D graphene devices by employing strain engineering. In particular, we focus on two structures: (i) single potential barriers with a finite strained graphene section inserted into the potential barrier region and (ii) graphene p–n junctions where strain is applied locally and symmetrically to both sides of the junction. An atomistic tight-binding model was used to describe the electronic transport through the devices. The Hamiltonian reads $H_{tb} = \Sigma_n U_n c_n^\dagger c_n + \Sigma_{nm} t_{nm} c_n^\dagger c_m$, where U_n stands for the potential energy at the nth site and t_{nm} is the nearest neighbor hopping energy between nth and mth sites. Under a uniaxial strain applied along the Ox direction, the C–C bond vectors change as[30,38]

$$\begin{cases} r_x(\sigma) \rightarrow (1+\sigma) r_x(0), \\ r_y(\sigma) \rightarrow (1-\gamma\sigma) r_y(0), \end{cases} \tag{1}$$

where σ is the strain amplitude and $\gamma = 0.165$ is the Poisson's ratio.[39] The hopping parameter between atoms is determined by $t_{nm}(\sigma) = t_0 \exp[-3.37(r_{nm}(\sigma)/r_0 - 1)]$ (Ref. 38) with $t_0 = -2.7\,\text{eV}$ and $r_{nm}(0) \equiv r_0 = 0.142\,\text{nm}$ being the hopping energy and the C-C distance in unstrained graphene, respectively. In general, there are three different hopping parameters $t_{1,2,3}$ corresponding to three bond vectors $r_{1,2,3}$, respectively, in the strained graphene region.[30] However, in this work, we consider the case where both the transport direction (Ox axis) and the direction of strain are parallel to the armchair line of graphene sheet so as to have a large transport gap for a given strain magnitude.[30] Therefore, there are only two different hopping parameters in strained graphene, i.e., $t_1 \equiv t_2$. Throughout the work, the transition zone of $\sim$10 nm between unstrained and strain sections (see Fig. 1) is considered.[30]

As in Refs. 30 and 45, to investigate the electronic transport properties of the devices, we employed the non-equilibrium Green's function formalism. Given the large mean free path of charge carriers with respect to the typical device size and low defect density achievable in high-quality graphene on appropriate substrate,[40–44] the scattering (i.e., on phonon, defects, etc.) is not expected to affect strongly

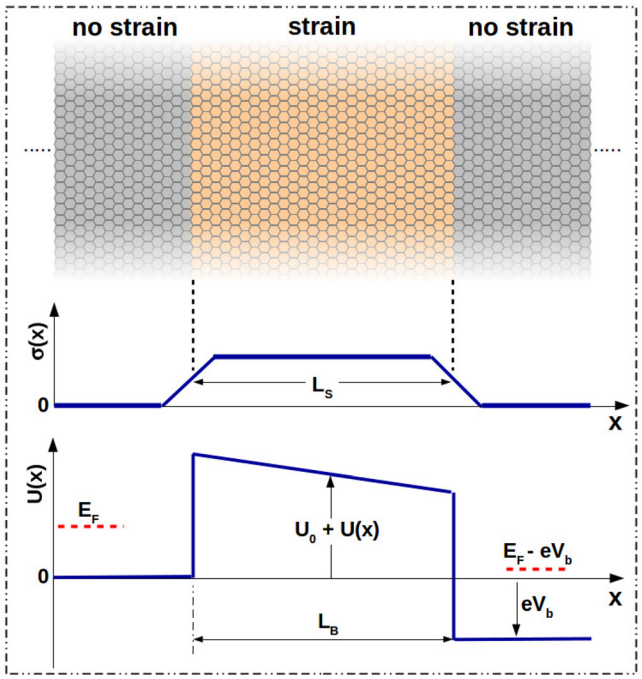

FIG. 1. Schematic of single potential barrier structures studied in this work. Strain is applied locally in an area of length L_S and the potential barrier of length L_B can be generated and controlled by an external gate voltage. The middle panel shows the strain profile $\sigma(x)$. The bottom one is the potential energy along the device channel when a bias voltage V_b is applied.

the physics of transport and the performance of the devices under investigation. On this basis, our simulations here were made in the ballistic approximation and the graphene channel was assumed to be free of defects and impurities. To this end, the tight-binding Hamiltonian H_{tb} is rewritten in the wavevector k_y-dependent (quasi-1D) form $H_{tb}(k_y)$.[30] The Green's function is then computed using the following equation:[47]

$$\mathcal{G}(\epsilon, k_y) = [\epsilon + i0^+ - H_{tb}(k_y) - \Sigma(\epsilon, k_y)]^{-1}, \tag{2}$$

where the self-energy $\Sigma(\epsilon, k_y) = \Sigma_L(\epsilon, k_y) + \Sigma_R(\epsilon, k_y)$ with $\Sigma_{L(R)}$ being the self-energies that describe the left (right) contact-to-device couplings. The transmission probability needed to evaluate the current is calculated as $\mathcal{T}_e(\epsilon, k_y) = \text{Tr}\{\Gamma_L \mathcal{G} \Gamma_R \mathcal{G}^\dagger\}$, with $\Gamma_{L(R)} = i(\Sigma_{L(R)} - \Sigma_{L(R)}^\dagger)$ being the transfer rate at the left (right) contact. The current density is obtained by the Landauer formula

$$J = \frac{e}{\pi h} \int_{BZ} dk_y \int d\epsilon \mathcal{T}_e(\epsilon, k_y) \{f_L(\epsilon) - f_R(\epsilon)\}. \tag{3}$$

In this expression, the integral over k_y is performed in the whole Brillouin zone and $f_{L(R)} = 1/[1 + \exp((E - E_{FL(R)})/k_B T)]$ are the Fermi distribution functions in the left (right) contact with the Fermi energies $E_{FL(R)}$. The local density of states (LDOS) is computed from the Green's function as $\mathcal{D}(\epsilon, k_y, \vec{r}_n) = -\text{Im}\{\mathcal{G}_{n,n}(\epsilon, k_y)\}/\pi$.[47]

III. RESULTS AND DISCUSSION

It has been shown that a small strain of a few percent cannot change the gapless character of pristine graphene, but

it causes the shift of Dirac points in k-space which may lead to dramatic changes of electronic transport features through strained graphene heterostructures.[30,46] For instance, the appearance of transport gap in unstrained/strained junctions, i.e., the vanishing of the conductance over a finite range of energy, has been observed.[30] Additionally, when a potential barrier is applied to the strained graphene regions, the energy band structure is shifted in energy. The combination of these shifts of graphene band structure both in k-space and in energy may lead to interesting features in the transport picture of single barrier structures as well as p–n tunnel diodes. In particular, not only does NDC behavior appear in these structures but the effect is also significantly enhanced even with a relatively small strain of a few percent. This will be demonstrated and discussed in detail below.

A. Single potential barrier structures

Important parameters that characterize the single potential barrier structure schematized in Fig. 1 are the length of strained region, L_S, the length of barrier, L_B, and the height of potential barrier, U_0, which can be generated and controlled by a gate electrode.[5–7] First, we display in Fig. 2 the I–V characteristics of the device with $L_S = L_B = 40$ nm calculated for different values of strain amplitude while the values of U_0 and Fermi energy E_F are kept fixed at 0.45 eV and 0.25 eV, respectively. The appearance of NDC effect is clearly shown and its behavior is, moreover, strongly dependent on strain amplitude. Without strain ($\sigma = 0$), the NDC effect is weak with the PVR being only marginally larger than 1 (see Fig. 2(a)). When strain is applied, the overall current is reduced as seen in Figs. 2(b) and 2(c) and the general trend is that the larger the strain amplitude, the smaller the overall current. However, the valley current decreases much more significantly than the peak current, leading to a strong increase of the PVR with strain amplitude. For instance, with a strain of 3%, PVR is slightly increased ($\sim$2–3), but it reaches a value of about 56 with a strain of 5%. Note that the increase of PVR is also strongly

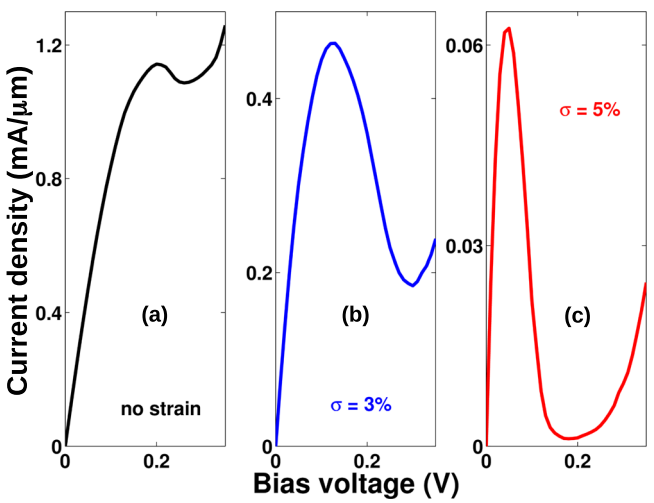

FIG. 2. I–V characteristics of a single potential barrier structure for different strain amplitudes. Other parameters of the structure are $L_S = L_B = 40$ nm, $U_0 = 0.45$ eV, and $E_F = 0.25$ eV.

dependent on other device parameters (i.e., U_0, E_F, and $L_{S,B}$) as discussed later. To explain the appearance of NDC effect in this structure and its enhancement when strain is applied, we display in Fig. 3 the $(E-k_y)$ maps of transmission probability at different values of bias voltage, V_b, for two cases: without strain (top panels, $\sigma = 0$) and with strain (bottom panels, $\sigma = 5\%$). The values of V_b for the two maps on the left panels are somehow arbitrarily chosen in the linear regions of I–V characteristics in Figs. 2(a) and 2(c), while those for the maps in the middle and right columns are the values corresponding to the peak and valley positions of the current, respectively.

Let us first recall the reason for the appearance of NDC effect for the case of pristine graphene (i.e., without strain). When increasing the bias voltage, the energy window between two Fermi energies, $[E_{FR}, E_{FL}]$, which provides the main contributions to the flow of current is widened, thus making the current larger as can be seen when comparing Figs. 3(a) and 3(b). However, increasing the bias voltage also causes the extension of the bottleneck effect[6,7] in the transmission probability (see Figs. 3(b) and 3(c)). When the bottlenecks of transmission probability enter into the energy window $[E_{FR}, E_{FL}]$, the current is reduced, which is the origin of the appearance of the NDC behavior observed in Fig. 2(a). It is noted that the bottleneck effect is still rather weak, hence the valley current cannot be completely/strongly suppressed. This explains the small PVR observed in the case of unstrained graphene devices.

When strain is applied, the picture of transmission probability is dramatically changed as seen in Figs. 3(d)–3(f). This can be understood from the schematics of energy band profile shown in Fig. 4. Essentially, when strain is applied, the Dirac points and band structure are shifted in k-space (dashed line) and hence the Klein tunneling can be strongly suppressed. This causes the appearance of a transport gap, E_g (see Fig. 4), in strained graphene junctions, the magnitude of which depends on the direction and amplitude of strain (see Ref. 30 for details), e.g., in the case considered here, E_g takes the values of 0.246 eV and 0.402 eV for a strain amplitude of 3% and 5%, respectively. Actually, this transport gap corresponds to the smallest energy interval where the Dirac cones of the strained and unstrained areas do not overlap. When a potential barrier of height U_0 is further applied in the strained graphene, the band structure is shifted upwards by the same energy amount. There are two possibilities here. If $U_0 < E_g$, the band structures of the two graphene sections overlap only in two regions (marked in red in Fig. 4(a)). However, when $U_0 > E_g$, there is another overlap region in the center, which corresponds to transitions between electron states outside the barrier and hole states in the barrier region. It is important to note that, in ballistic transport regime, the transmission probability can get a finite value only in these overlap regions. This explains for the map of transmission probability at low bias voltage (Fig. 3(d)). Among the three overlap regions, only the middle one can be strongly modulated, i.e., it can be suppressed completely when increasing the bias voltage (Figs. 3(e) and 3(f)). Thus, this middle region plays a decisive role in the occurrence of NDC effect, while the contribution of other regions always makes the

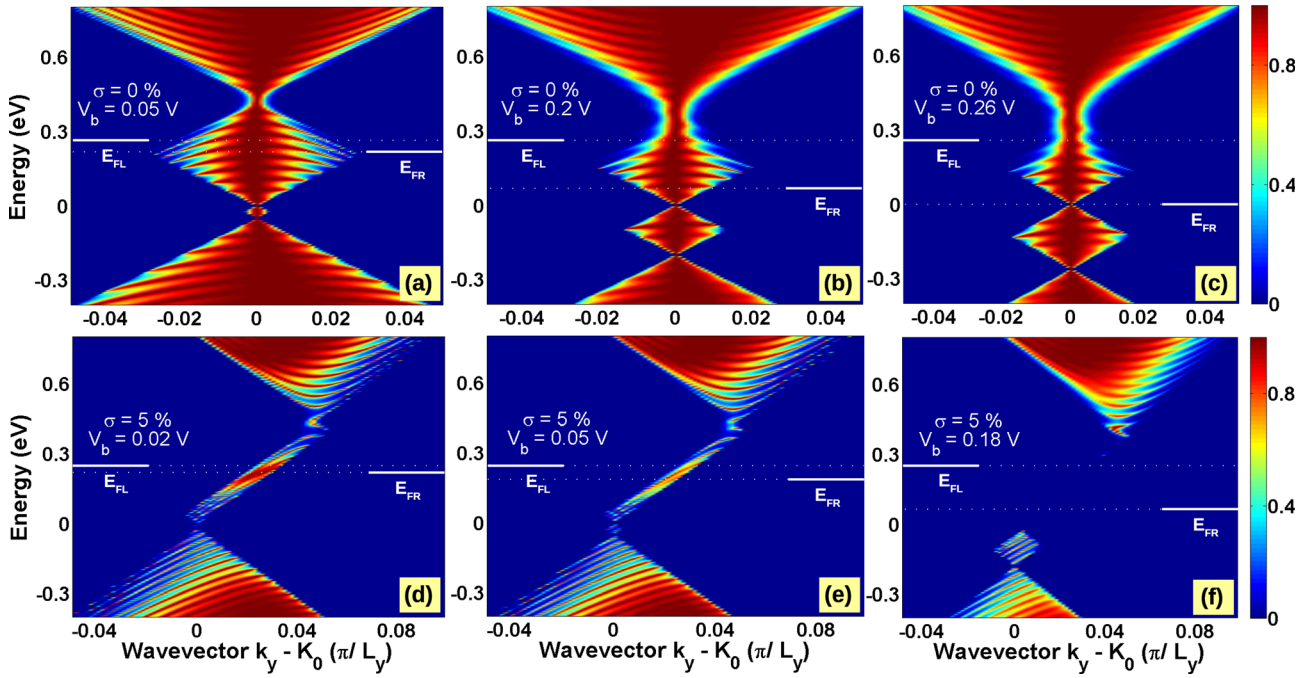

FIG. 3. (E–k_y) maps of transmission probability in two cases of unstrained (top) and strained (bottom) devices with different applied bias. K_0 denotes the position of Dirac point of unstrained graphene and $U_0 = 0.45$ eV is considered here.

current increase with the bias. Indeed, it is clearly seen that the transmission probability in the energy window [E_{FR}, E_{FL}] is largely reduced (even to zero as in Fig. 3(f)). This effect, on one hand, reduces the overall current, but, on the other hand, leads to a significant increase of PVR due to the strong suppression of valley current.

To investigate the dependence of NDC behavior on the barrier height, U_0, and Fermi level, E_F, we plot (E_F–U_0) maps of peak current (Fig. 5(a)) and PVR (Fig. 5(b)) for a strain of 5%. The result shows that NDC effect does not appear in two regions where U_0 is low (regardless of the value of Fermi energy) or U_0 is high and E_F is small. It is noted that here we only consider $E_F \leq 0.4$ eV, i.e., in the range corresponding to realistic doping concentrations. The disappearance of NDC in the region of small U_0 ($U_0 < E_g$) is due to the fact that at zero bias, the two band structures do not overlap in the middle region as discussed above and illustrated in Fig. 4(a). For higher U_0 ($U_0 > E_g$), there are three overlap regions and it is convenient to decompose the current into two components as

$$J_{tot} = J_{mid} + J_{other}, \tag{4}$$

where J_{mid} is the contribution from the middle region and J_{other} is due to the top and bottom regions. Note that while J_{mid} can be reduced, J_{other} always increases when raising the bias. At high bias, J_{other} dominates and hence the current always increases with the bias. For small Fermi energies, this is also true in the region of low bias and, hence, NDC behavior cannot be observed in these cases. The situation changes when E_F is larger, i.e., the contribution of the middle region, J_{mid}, becomes more important in the low bias region and thus the NDC effect occurs. Moreover, the higher the potential barrier U_0 the larger the middle overlap region, i.e., the larger the peak current, as can be seen in Fig. 5(a). However, the valley current is also high in this case because the middle region is so large that it cannot be completely suppressed at the low bias while, as mentioned, the component J_{other} can have an important contribution to J_{tot} when raising the bias. This explains the fact that the maximum of PVR occurs in the region with moderate U_0 and E_F in Fig. 5(b). Therefore, the moderate values of barrier height and Fermi level are the best compromise to have a high PVR, while the peak current is still large, e.g., $U_0 \cong 0.45$ eV and $E_F \cong 0.25$ eV in Fig. 2(c).

Another important parameter that can affect the NDC behavior of the considered device is the length of strained region, L_S. In our study, we always keep L_S equal to the length of barrier region, L_B, to avoid the complication arising from other unstrained/strained junctions when these two lengths are not equal. It is worth to note that in the case where $L_S \neq L_B$, one can anticipate that the NDC behavior is

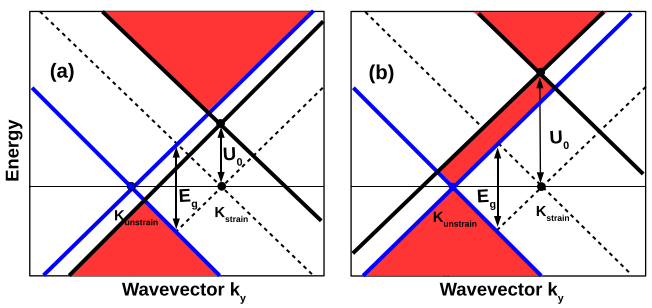

FIG. 4. Schematics of graphene band profile illustrating the shift of Dirac cone along k_y axis (due to strain) and in energy (due to potential barrier U_0) when $U_0 < E_g$ (a) and $U_0 > E_g$ (b) where E_g is the transport gap obtained for $U_0 = 0$. The blue lines are the bandedges in unstrained graphene, while the (dashed/solid) black lines are the bandedges (for $U_0 = 0/U_0 > 0$) in strained graphene. $K_{unstrain}$ and K_{strain} denote the positions of Dirac point in the k_y axis in these two cases, respectively.

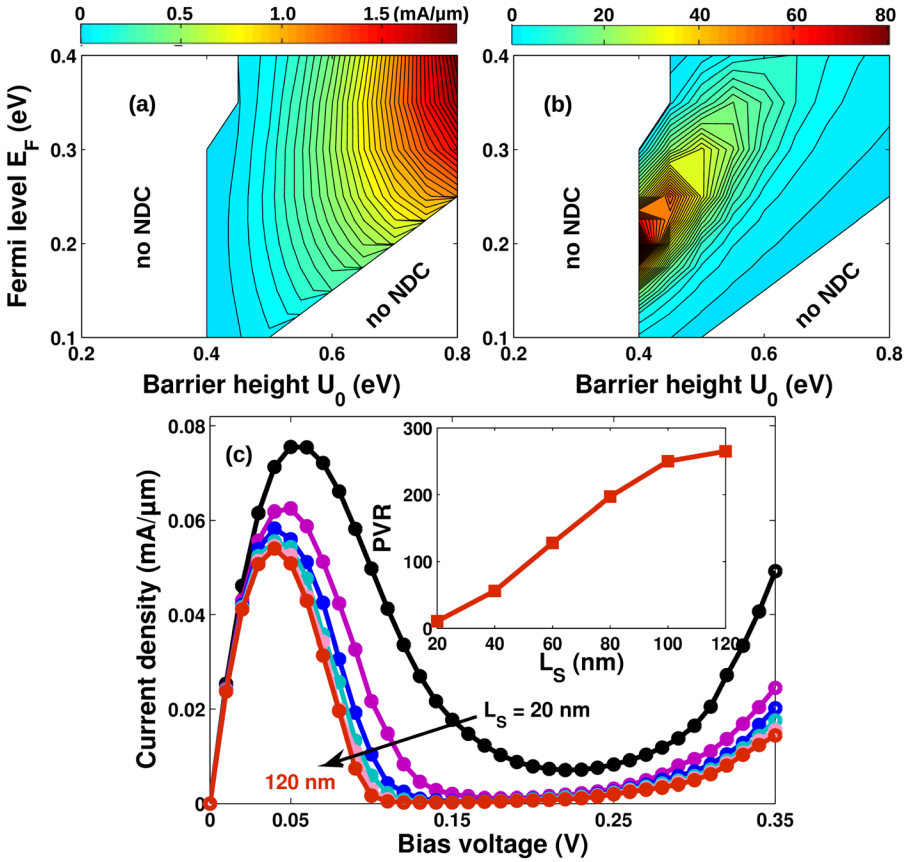

FIG. 5. (E_F-U_0) maps of peak current (a) and PVR (b) in the single potential barrier structure with $L_S = L_B = 40$ nm and $\sigma = 5\%$. (c) I–V characteristics computed for different lengths of strained region L_S. The inset shows the PVR as a function of L_S. Other parameters are $E_F = 0.25$ eV, $U_0 = 0.45$ eV, and $\sigma = 5\%$.

still observed, but the transport gaps resulting from the complicated profile of junctions should affect the peak current. The I–V characteristics obtained using $U_0 = 0.45$ eV, $E_F = 0.25$ eV, and $\sigma = 5\%$ with different values of L_S are displayed in Fig. 5(c). The general trend is that increasing L_S leads to a decrease in overall current, but the valley current is suppressed much more significantly than the peak current. This is due to the fact that both propagating and evanescent states contribute to the latter, while the former has contributions from evanescent states only. As a consequence, the PVR increases with L_S and can reach a value of a few hundred when L_S is of the order of 100 nm as can be seen in the inset of Fig. 5(c). It is noted, however, that this trend is only valid in the limit of ballistic approximation, i.e., if L_S is less than a few hundred nm.[40–44] When the device length is too large, the current can be affected by scatterings, which is predicted to reduce the peak current and hence the PVR.

B. p–n junctions

It is known that opening a bandgap in graphene is also a key ingredient to have a strong NDC behavior in graphene p–n devices. Indeed, several proposals based on this strategy have been investigated previously, e.g., in Refs. 13, 27, and 28. In this section, we will show that a significant enhancement of NDC effect in graphene p–n junctions can also be achieved by applying a local strain in the active region of the device channel. A schematic of the structure under study is shown on the top panel of Fig. 6, where p-doped and n-doped regions can be generated by electrostatic[48] or by chemical doping.[49] The structure is

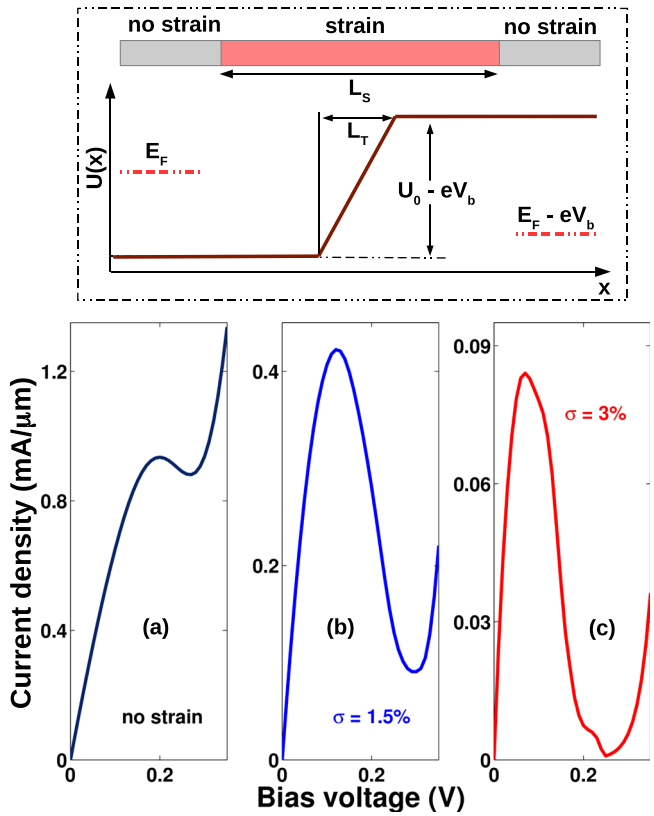

FIG. 6. The top panel shows the model of graphene p–n junctions studied in this work. The bottom panel shows the I–V characteristics obtained with different strain amplitudes. Other parameters of the device are $U_0 = 0.5$ eV, $L_S = 40$ nm, and $L_T = 10$ nm.

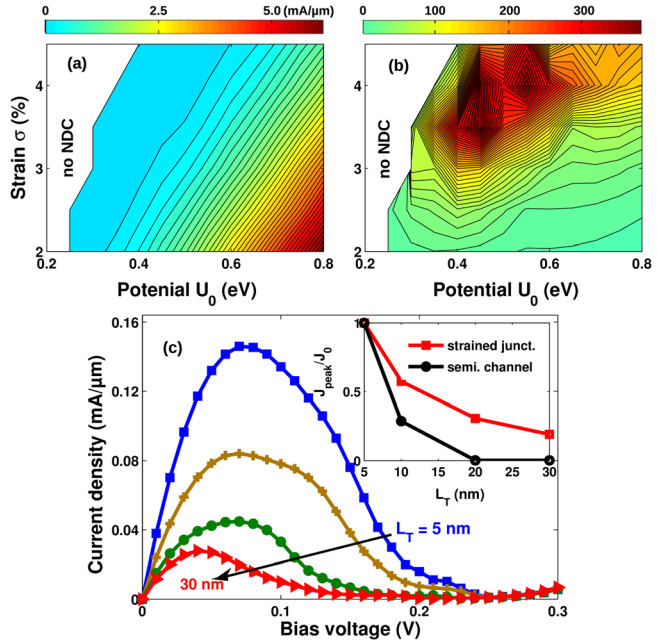

FIG. 7. (σ–U_0) maps of peak current (a) and PVR (b) in the p–n junction with $L_S = 40$ nm and $L_T = 10$ nm. (c) I–V characteristics of the device with different lengths L_T, while $L_S = 40$ nm is fixed. The inset shows the evolution of peak current J_{peak} when increasing L_T, compared with that in the case of normal semiconducting (gapped) graphene channel, where J_0 is the current obtained for $L_T = 5$ nm. Other parameters in (c) are $\sigma = 3\%$ and $U_0 = 0.5$ eV.

characterized by the potential difference, U_0, the length of strain area, L_S, and the length of transition region, L_T. It is noted that L_S must be considerably larger than L_T so as to generate two strained/unstrained junctions, i.e., one in each doping section.[45]

The enhancement of NDC behavior due to local strain is demonstrated in the bottom panel of Fig. 6, where I–V characteristics of a p–n junction with $L_S = 40$ nm and $L_T = 10$ nm calculated for different strain amplitudes are displayed. Not surprisingly, the NDC behavior is weak in the junction without strain ($\sigma = 0$), while the effect is enhanced significantly when strain is applied. Remarkably, PVR can reach a value of 100 for a small strain of 3%. The enhancement of NDC effect can be understood noting that the two unstrained/strained junctions formed in the channel create two different energy gaps in the transmission function.[45] The energy window between the gaps has a non-zero transmission probability due to the band-to-band tunneling (BTBT) that provides an important contribution to the current. When raising the bias voltage, this energy window is narrowed and the BTBT contribution to the current is reduced. This is the origin of the NDC behavior observed in this device.

Now, we investigate the effect of changing some device parameters on the NDC behavior of the structure. In Figs. 7(a) and 7(b), we plot the maps of peak current and PVR for different strain amplitudes and potential differences. In the range of strain amplitude considered here, the NDC behavior is not observed in the regime of low potential difference, i.e., $U_0 \lesssim 0.25$ eV, because there is no BTBT current in this case.[45] The dependence of peak current and PVR on strain and potential are rather complex. For instance, while the peak current is large in the region with high U_0 and small σ, the maximum of PVR, which depends on both the peak and valley currents, occurs a moderate potential height and a large strain. Therefore, we suggest to use moderate values of strain and potential, such as, for instance, $\sigma = 3\%$ and $U_0 = 0.5$ eV, to obtain a high PVR with a still large peak current in this structure.

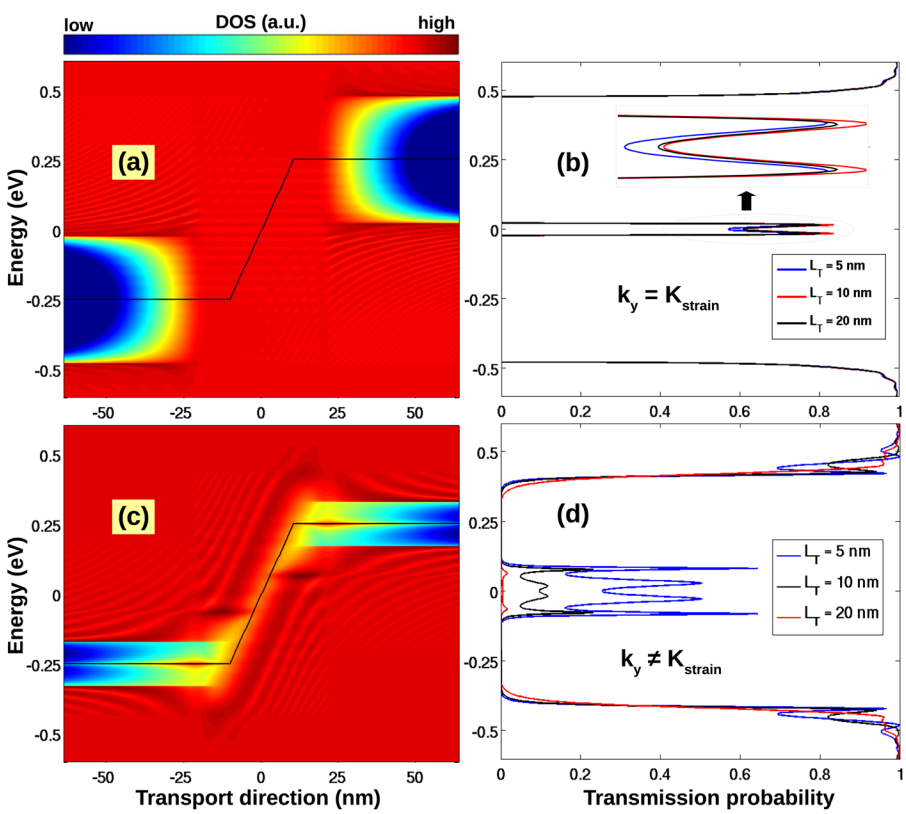

FIG. 8. Maps of local density of states (left) and corresponding transmission probability (right) obtained for two different wavevectors k_y. In the right side, devices with different lengths L_T are considered. The inset in (b) shows a zoomed image of the transmission probability around the zero energy point. Other device parameters are $L_S = 40$ nm, $\sigma = 3\%$, and $U_0 = 0.5$ eV.

It has been shown that the peak current in the p-n devices made of simple semiconducting materials is very sensitive to the length of transition region L_T.[27,28] Therefore, we examine, in Fig. 7(c), the *I–V* characteristics at different lengths L_T while keeping the value of L_S fixed at 40 nm (the above mentioned optimized values of strain and potential were used). It is clearly shown that, because of the decrease of BTBT current, the peak current is reduced when increasing L_T. However, the decrease of peak current in the structure considered here is not very strong compared with other p–n junction devices made of a simple gapped graphene channel as seen in the inset of Fig. 7(c). As a result, the PVR is weakly degraded when increasing L_T, namely, PVR is about 148 for $L_T = 5$ nm and reduces slightly to ~100 for $L_T = 30$ nm. To explain this weak sensitivity of the peak current to L_T, we display in Fig. 8 the maps of LDOS and the transmission probability for two different modes k_y. For the mode $k_y = K_{strain}$, i.e., corresponding to the position of a Dirac point in the strained section, the BTBT current is less sensitive to L_T (Fig. 8(b)) due to the zero bandgap in the transition region as seen in Fig. 8(a). For the other mode where k_y is far from K_{strain} (Fig. 8(c)), the BTBT is strongly reduced as shown in Fig. 8(d) because the gap in the transition region is finite. It is the contribution of modes around K_{strain} that makes the peak current less sensitive to L_T, compared with the case of devices made of uniform gapped graphene channels. Hence, the PVR here is not strongly degraded when increasing L_T.

IV. CONCLUSION

In this work, we have shown that due to the effects of local strain, the Klein tunneling is strongly suppressed and hence a transport gap can occur in the graphene channels with strained/unstrained junctions. This gap can be modulated in *k*-space and in energy by strain and doping engineering, respectively. Thanks to this effect, a strong NDC can be achieved in the considered graphene devices (single gate-induced barrier and p–n structures) when a local strain is suitably applied. Remarkably, with a small strain of a few percent, the PVR can reach a value of a few hundred at room temperature. The dependence of NDC behavior on the device parameters has been systematically analyzed. It is shown that a strong NDC effect can be achieved in single barrier structures with large strain area, while it is not strongly sensitive to the change in the length of transition region in p–n devices. These results suggest that strain engineering can be a promising way to overcome the lack of bandgap in graphene and to enlarge the route towards high-performance graphene-based electronic devices.

ACKNOWLEDGMENTS

This research in Hanoi was funded by Vietnam's National Foundation for Science and Technology Development (NAFOSTED) under Grant No. 103.01-2014.24.

[1]H. Mizuta and T. Tanoue, *The Physics and Applications of Resonant Tunneling Diodes* (Cambridge University Press, Cambridge, 1995).
[2]Y. Wu, V. Perebeinos, Y.-M. Lin, T. Low, F. Xia, and P. Avouris, Nano Lett. **12**, 1417–1423 (2012).
[3]K. Majumdar, S. Kallatt, and N. Bhat, Appl. Phys. Lett. **101**, 123505 (2012).
[4]Y. Wu, D. B. Farmer, W. Zhu, S. J. Han, C. D. Dimitrakopoulos, A. A. Bol, P. Avouris, and Y.-M. Lin, ACS Nano **6**, 2610–2616 (2012).
[5]P. Sharma, L. S. Bernard, A. Bazigos, A. Magrez, and A. M. Ionescu, ACS Nano **9**, 620–625 (2015).
[6]A. Alarcón, V. H. Nguyen, S. Berrada, D. Querlioz, J. Saint-Martin, A. Bournel, and P. Dollfus, IEEE Trans. Electron Devices **60**, 985–991 (2013).
[7]R. Grassi, T. Low, A. Gnudi, and G. Baccarani, IEEE Trans. Electron Devices **60**, 140–146 (2013).
[8]D. Dragoman and M. Dragoman, Appl. Phys. Lett. **90**, 143111 (2007).
[9]V. N. Do, V. H. Nguyen, P. Dollfus, and A. Bournel, J. Appl. Phys. **104**, 063708 (2008).
[10]L. Britnell *et al.*, Nat. Commun. **4**, 1794 (2013).
[11]A. Mishchenko *et al.*, Nat. Nanotechnol. **9**, 808–813 (2014).
[12]Y. Zhao, Z. Wan, X. Xu, S. R. Patil, U. Hetmaniuk, and M. P. Anantram, Sci. Rep. **5**, 10712 (2015).
[13]G. Fiori, IEEE Electron Device Lett. **32**, 1334–1336 (2011).
[14]J. Milton Pereira, Jr., P. Vasilopoulos, and F. M. Peeters, Appl. Phys. Lett. **90**, 132122 (2007).
[15]Y. Song, H. C. Wu, and Y. Guo, Appl. Phys. Lett. **102**, 093118 (2013).
[16]I. Rodríguez-Vargas, J. Madrigal-Melchor, and O. Oubram, J. Appl. Phys. **112**, 073711 (2012).
[17]V. H. Nguyen, F. Mazzamuto, A. Bournel, and P. Dollfus, J. Phys. D: Appl. Phys. **45**, 325104 (2012).
[18]G. J. Ferreira, M. N. Leuenberger, D. Loss, and J. Carlos Egues, Phys. Rev. B **84**, 125453 (2011).
[19]H. Ren, Q. X. Li, Y. Luo, and J. Yang, Appl. Phys. Lett. **94**, 173110 (2009).
[20]H. Teong, K. T. Lam, S. B. Khalid, and G. Liang, J. Appl. Phys. **105**, 084317 (2009).
[21]J. W. González, M. Pacheco, L. Rosales, and P. A. Orellana, Phys. Rev. B **83**, 155450 (2011).
[22]S. Li, C. K. Gan, Y.-W. Son, Y. P. Feng, and S. Y. Quek, Appl. Phys. Lett. **106**, 013302 (2015).
[23]A. Cresti, G. Grosso, and G. P. Parravicini, Phys. Rev. B **77**, 233402 (2008).
[24]Z. F. Wang, Q. Li, Q. W. Shi, X. Wang, J. Yang, J. G. Hou, and J. Chen, Appl. Phys. Lett. **92**, 133114 (2008).
[25]V. N. Do and P. Dollfus, J. Appl. Phys. **107**, 063705 (2010).
[26]H. Cheraghchi and H. Esmailzade, Nanotechnology **21**, 205306 (2010).
[27]V. Hung Nguyen, F. Mazzamuto, J. Saint-Martin, A. Bournel, and P. Dollfus, Appl. Phys. Lett. **99**, 042105 (2011).
[28]V. Hung Nguyen, F. Mazzamuto, J. Saint-Martin, A. Bournel, and P. Dollfus, Nanotechnology **23**, 065201 (2012).
[29]K. S. Kim *et al.*, Nature **457**, 706–710 (2009).
[30]M. C. Nguyen, V. H. Nguyen, H. V. Nguyen, and P. Dollfus, Semicond. Sci. Technol. **29**, 115024 (2014).
[31]W. Bao *et al.*, Nat. Nanotechnol. **4**, 562–566 (2009).
[32]T. Q. Trung *et al.*, Adv. Funct. Mater. **24**, 117–124 (2014).
[33]C. Metzger *et al.*, Nano Lett. **10**, 6–10 (2010).
[34]C. N. Lau, W. Bao, and J. Velasco, Jr., Mater. Today **15**, 238–245 (2012).
[35]J. Li, T.-F. Chung, Y. P. Chen, and G. J. Cheng, Nano Lett. **12**, 4577–4583 (2012).
[36]A. Castellanos-Gomez *et al.*, Nano Lett. **13**, 5361–5366 (2013).
[37]S. Yang *et al.*, Nano Lett. **15**, 1660–1666 (2015).
[38]V. M. Pereira, A. H. Castro Neto, and N. M. R. Peres, Phys. Rev. B **80**, 045401 (2009).
[39]O. L. Blakslee, D. G. Proctor, E. J. Seldin, G. B. Stence, and T. Wen, J. Appl. Phys. **41**, 3373 (1970).
[40]R. Decker *et al.*. Nano Lett. **11**, 2291–2295 (2011).
[41]J. Xue *et al.*, Nat. Mater. **10**, 282–285 (2011).
[42]P. J. Zomer *et al.*, Appl. Phys. Lett. **99**, 232104 (2011).
[43]A. S. Mayorov *et al.*, Nano Lett. **11**, 2396–2399 (2011).
[44]K. I. Bolotin *et al.*, Solid State Commun. **146**, 351–355 (2008).
[45]M. C. Nguyen, V. H. Nguyen, H. V. Nguyen, J. Saint-Martin, and P. Dollfus, Physica E **73**, 207–212 (2015).
[46]D. A. Bahamon and V. M. Pereira, Phys. Rev. B. **88**, 195416 (2013).
[47]M. P. Anantram, M. S. Lundstrom, and D. E. Nikonov, Proc. IEEE **96**, 1511–1550 (2008).
[48]D. B. Farmer, Y.-M. Lin, A. Afzali-Ardakani, and P. Avouris, Appl. Phys. Lett. **94**, 213106 (2009).
[49]J. R. Wiliams, L. DiCarlo, and C. M. Marcus, Science **317**, 638 (2007).